Block copolymer nanopatterns affect cell spreading: stem versus cancer bone cells

R. Fontelo, D. Soares da Costa, R.L. Reis, R. Novoa-Carballal, I. Pashkuleva

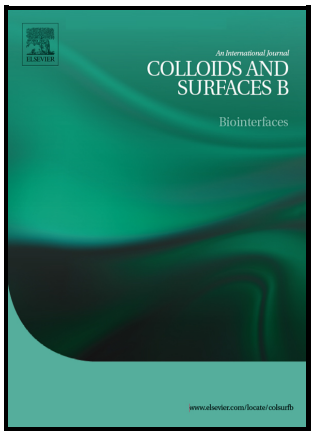

PII: S0927-7765(22)00457-X

DOI: https://doi.org/10.1016/j.colsurfb.2022.112774

Reference: COLSUB112774

To appear in: *Colloids and Surfaces B: Biointerfaces*

Received date: 9 May 2022
Revised date: 5 August 2022
Accepted date: 10 August 2022

Please cite this article as: R. Fontelo, D. Soares da Costa, R.L. Reis, R. Novoa-Carballal and I. Pashkuleva, Block copolymer nanopatterns affect cell spreading: stem versus cancer bone cells, *Colloids and Surfaces B: Biointerfaces,* (2022) doi:https://doi.org/10.1016/j.colsurfb.2022.112774

Block copolymer nanopatterns affect cell spreading: stem versus cancer bone cells

R. Fontelo[a,b], D. Soares da Costa[a,b], R. L. Reis[a,b], R. Novoa-Carballal[,a,b], I. Pashkuleva[*a,b]*

[a] 3B's Research Group, I3Bs – Research Institute on Biomaterials, Biodegradables and Biomimetics, University of Minho, Headquarters of the European Institute of Excellence on Tissue Engineering and Regenerative Medicine, AvePark, Parque de Ciência e Tecnologia, Zona Industrial da Gandra, 4805-017 Barco, Portugal;

[b] ICVS/3B's–PT Government Associate Laboratory, Braga/Guimarães, Portugal.

Abstract

Bone healing after a tumor removal can be promoted by biomaterials that enhance the bone regeneration and prevent the tumor relapse. Herein, we obtained several nanopatterns by self-assembly of polystyrene-block-poly 2-vinyl pyridine (PS-*b*-P2VP) with different molecular weight and investigated the adhesion and morphology of human bone marrow mesenchymal stem cells (BMMSC) and osteosarcoma cell line (SaOS-2) on these patterns aiming to identify topography and chemistry that promote bone healing. We analyzed > 2000 cells per experimental condition using imaging software and different morphometric descriptors, namely area, perimeter, aspect ratio, circularity, surface/area, and fractal dimension of cellular contour (FDC). The obtained data were used as inputs for principal component analysis, which showed distinct response of BMMSC and SaOS-2 to the surface topography and chemistry. Among the studied substrates, micellar nanopatterns assembled from the copolymer with high molecular weight promote the adhesion and spreading of BMMSC and have an opposite effect on SaOS-2. This nanopattern is thus beneficial for bone regeneration after injury or pathology, e.g. bone fracture or tumor removal.

Graphical abstract

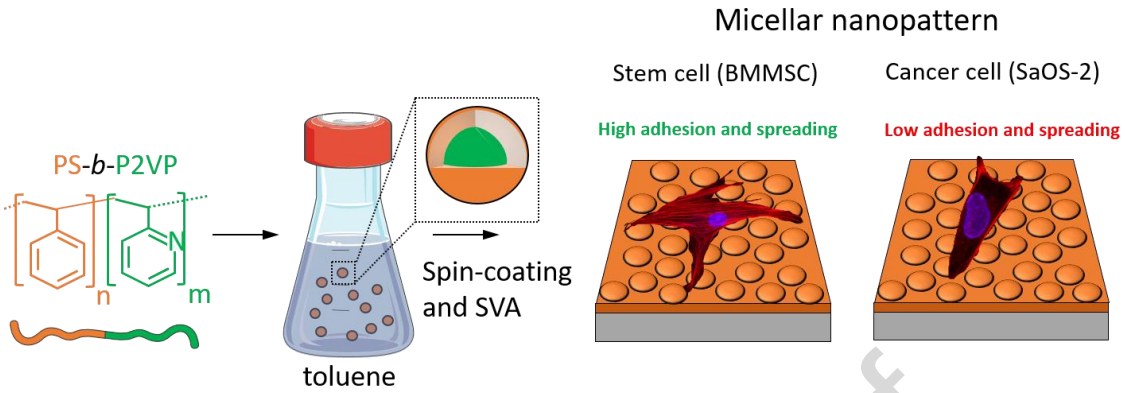

Keywords

Nanopattern, Block copolymer, Coating, Stem Cell, Cancer Cell

1. Introduction

Most tissue-derived cells are anchorage-dependent, *i.e.* they need to adhere in order to survive, proliferate, migrate, and differentiate.[1] Cells adhesion is mediated by surface receptors such as integrins, cadherins, and selectins that act as signal transducers between the cells and their environment. As an example, these receptors are main players in the development of adhesion points that are connected with the intracellular actin and thus, contribute to the assembly and reorganization of the cytoskeleton.[2] The modulation of the adhesion process is therefore a way to control cell morphology and consequently cell behavior.[3, 4]

In tissue engineering and regenerative medicine, a common strategy to achieve such control is the use of substrate/implant with surface properties that promote cell adhesion, tissue regeneration/formation and integration. Alternatively coating of the device with a thin layer that has such pro-adhesive properties can be applied. Nanotechnology has provided different tools for tuning surface topography[5-7] and chemistry[8, 9] toward optimal interactions with cells surface receptors leading to a targeted cells response.[10-12] There is a wide variety of methods that can be used to obtain different nanotopography, *e.g.* etching, nanoparticle deposition, phase separation, or molecular self-assembly can result in surfaces with isotropic nanoroughness, nanogrooves, nanofibers, or nanopillars that evoke different cell response.[13-21] Among these methods, block copolymer (BCP) self-assembly has

several advantages: it can be applied to large surface areas, it allows for high (nanoscale) spatial resolution, the surface chemistry can be tuned by selecting the monomers, while the topography can be tailored by changing the molecular weight of the blocks and the processing conditions.[22]

We and others have demonstrated that BCP nanopatterns generated from polystyrene-block-poly(2-vinyl pyridine) (PS-*b*-P2VP) are stable at physiological conditions and sustain human cells viability. [23, 24] Previous data have also shown that such nanopatterns have bactericidal properties that depend on their topography and chemistry.[24] These studies have indicated the potential of BCP nanopatterns for tissue engineering, regeneration, and healing applications as well as the possibility to tailor the cell adhesion and morphology *via* an adjustment of the pattern topography. Herein, we investigated the behavior of two osteo related cells types, namely bone marrow mesenchymal stem cells (BMMSC) and osteoblasts-like cells (SaOS-2) cultured in contact with PS-*b*-P2VP nanopatterns with different topography. Considering a scenario of implantation that targets bone regeneration/healing and requires a prompt adhesion, *i.e.* implies that the adhering cells will begin to perform their function earlier[25, 26], we have performed a detailed multi-parametric analysis of cell adhesion and morphology changes over 24 h. This analysis demonstrated a distinct behavior of each cell type cultured on the nanostructures.

2. Materials and Methods

2.1. Materials and reagents

Polystyrene-*block*-poly(2-vinyl pyridine) (PS-*b*-P2VP) was purchased from Polymer Source, Inc (Quebec, Canada). Polymers with different weight-average molecular weights (Mw) of the paired blocks were used, namely PS_{127}-*b*-$P2VP_{92}$ and PS_{320}-*b*-$P2VP_{398}$, where the subscripts correspond to the Mw of each block in kDa. The polydispersity index Mw/Mn (where Mn is number-averaged molecular weights) for these polymers were 1.10 and 1.25, respectively. Squared glass coverslips (20x20 mm) were purchased from Carl Roth. Chloroform and toluene were purchased from Fisher-Chemical. ALNOCHORMIX™, Histopaque density gradient, α-MEM, DMEM and phalloidin-TRITC were ordered from Sigma-Aldrich. Antibiotic/antimycotic

(streptomycin and penicillin), fetal bovine serum (FBS, South American) and TrypLE express were purchased from Gibco, and DAPI was acquired from Invitrogen.

2.2. Methods

2.2.1. Preparation of the nanopatterns

The block copolymers (1 or 2 wt%) were stirred in toluene overnight at room temperature, filtered (0.22 μm PTFE filter), and used to spin-coat glass coverslips (3000 rpm during 40 s). Glass coverslips were previously washed by immersing them in a sulfuric acid solution of ALNOCHORMIX™ following the manufacturer indications overnight, rinsed with water and dried with a nitrogen stream. The coated substrates were submitted to a solvent vapor annealing (SVA) for 3 h at 50 % of humidity and a temperature between 20 and 25 °C. Toluene or chloroform were used as solvents for the SVA process.[24] After SVA, the substrates were dried under a N_2 stream to evaporate any residual solvent. The generated nanopatterns were characterized by atomic force microscopy (AFM, DIMENSION icon, Bruker) using the PeakForce™ Taping mode (cantilevers with a spring constant of 0.4 N/m and frequency of 70 Hz). Topography and roughness were measured using the NanoScope Analysis 1.5 software. The surface wettability was determined by the sessile drop method using an OCA 15+ equipment (DataPhysics) and water (3 μL) as a testing liquid. To identify the surface-exposed polymer blocks, the substrates were immersed in an acidic solution of gold salts (10 mM $HAuCl_4$ in 0.9 % HCl (aq.), the gold has an affinity to the P2VP) and analyzed by AFM.[24]

2.2.2. Cell culture and analysis

Human bone marrow aspirates were obtained from healthy patients under the agreement with the Hospital da Prelada (Porto, Portugal). Human bone marrow mesenchymal stem cells (BMMSC) were separated using a Histopaque density gradient (1.077 g/mL) and washed with phosphate buffered saline (PBS). BMMSC (passages 2-5) were expanded in α-MEM supplemented with 1 % antibiotic/antimycotic and 10 % FBS. Osteosarcoma cells (ATCC, USA, SaOS-2, passages 15-20) were cultured in DMEM supplemented with 1 % antibiotic/antimycotic and 10 % FBS. Cells were detached from the tissue culture polystyrene with TrypLE express after achieving 70 % of confluence

and seeded on the nanopatterns at a density of 5000 cells/cm^2 using the respective medium (α-MEM for BMMSC culture and DMEM for SaOS-2). We used serum free media to avoid the concealment of the nanopatterns by the serum proteins.[27, 28]. The cultures were incubated (37 °C, 5 % CO_2) and cells (2000-5000 cells/sample) were analyzed at three timepoints (1, 7 and 24 h). Prior the analysis, the media was aspirated, the substrates with the adhered cells were washed twice with PBS to remove the non-adherent cells and fixed with 10 % formalin. The cells were incubated with phalloidin-TRITC (1:100) for morphology analysis, while staining with DAPI (1:500) was used to determine the attached cells. Images were taken with a fluorescence microscope (Inverted Microscope Axio Observer) with a 10x objective, acquiring tiles of the whole sample to represent the heterogeneity in the cell population.[29] Cells count and morphology analysis were performed with Fiji (Image J 2.3.0). A threshold was applied to each channel to discard background pixels. With the tool "analyze particles," the size range was defined to avoid quantifying small debris from cells that did not adhere and groups of cells, including only the size of individual cells on the final range. To assess any morphological changes, we have analyzed each cell projected area, perimeter, aspect ratio (AR=major axis/minor axis, *i.e.* higher values indicate more elongated cells) and the circularity ((4π x area)/perimeter^2, where a value of 1 indicates a perfect circle). All experiments were repeated three times with four replicates. TCPS was used as a control substrate.

2.2.3. Statistical analysis

Statistical analysis was performed with GraphPad Prism 9 software. Shapiro-Wilk test ($p < 0.05$) was used to evaluate the normality of the data. When the data did not follow the normal distribution, an initial Kruskal-Wallis test was followed by a Dunn's multiple comparison test.

2.2.4. Principal component analysis (PCA)

The obtained morphometric data for the area, perimeter, AR and circularity of the cells were used as inputs for PCA. We have included two extra morphometric parameters that can be obtained from the original morphometric data, surface-area (SA = Perimeter/Area) and Fractal dimension of cellular contour (FDC =

2*log(Perimeter)/log (Area)). Area and perimeter were considered as size descriptors, while AR, circularity, SA and FDC as shape descriptors. PCA was performed in R (RStudio 2021.09.1 Build 372). The results were plotted in the PCA biplot using standardized PC1 and PC2 for each cell type. The adhesion parameters (variables) were plotted as eigenvectors.

3. Results and discussion

3.1. *Nanopattern preparation and characterization*

Cell adhesion is a crucial process in the fixation and integration of prosthesis, *e.g.,* for bone repair. Increased surface area of the nanotopographies facilitates this process. Moreover, certain topographies such as nanogrooves and nanopillars can promote osteogenic differentiation.[16-18] The topography alone or in combination with chemical cues (*e.g.* bioactive peptides, chemokines or antibodies) can also induce cell-type selectivity, *i.e.* can enhance the adhesion of a targeted cell type over others.[19-21]

To develop different nanotopographies, we have used the block copolymer PS-*b*-P2VP, known for its self-assembly ability and possibility for posterior reorganization of the formed pattern by a solvent vapor annealing (SVA).[30] SVA is performed in a saturated atmosphere of solvent that reduces the glass transition temperature of the block polymers in function of their affinity to the used solvent, thus, enhancing polymer chain mobility and allowing reorganization.[30] Previous study by Khor *et al.* showed that micellar and worm-like nanopatterns generated from PS-*b*-P2VP and PS-*b*-P4VP promote different cell adhesion: preferential adhesion of either fibroblast or BMMSC was observed onto worm-like cylindrical nanopatterns when compared to micellar patterns.[23] Although the comparison between the different patterns is obscured because of the use of two different polymers for the pattern preparation and the number of analyzed cells was limited, this study suggests that BCP nanopatterns can be good substrates to control cell adhesion without bio-functionalization.

Herein, we generated four different nanopatterns by using the same block copolymer, PS-*b*-P2VP, but varying the molecular weight of the blocks and the solvent used for SVA (Fig. 1). PS and P2VP blocks have different solubility in the used SVA solvents: toluene is a good solvent for PS and SVA in toluene results in an assembly of

micellar structures with surface-exposed PS and a P2VP inner core (Fig. 1A). On the other hand, chloroform is a good solvent for both blocks and the generated nanopatterns have PS and PV2P exposed at the surface.[24, 31] Previously, we have shown that the patterns generated by SVA in chloroform are composed by lamellae and cylinders arranged vertically to the surface in the case of PS_{127}-*b*-$P2VP_{92}$. For this pattern, the P2VP is located in the ridges. In the case of PS_{320}-*b*-$P2VP_{398}$, the patterns generated at the same conditions are most likely perforated lamellas, and the P2VP is found in the valleys (demonstrated by PV2P staining with gold).[31] As expected, the micelles or polymer domains (in the cylinders and lamellae) are bigger for the PS_{320}-*b*-$P2VP_{398}$ than for PS_{127}-*b*-$P2VP_{92}$ (Fig. 1B vs 1C, Table S1). The water contact angle for all generated patterns was similar, *i.e.* about 85 degrees.

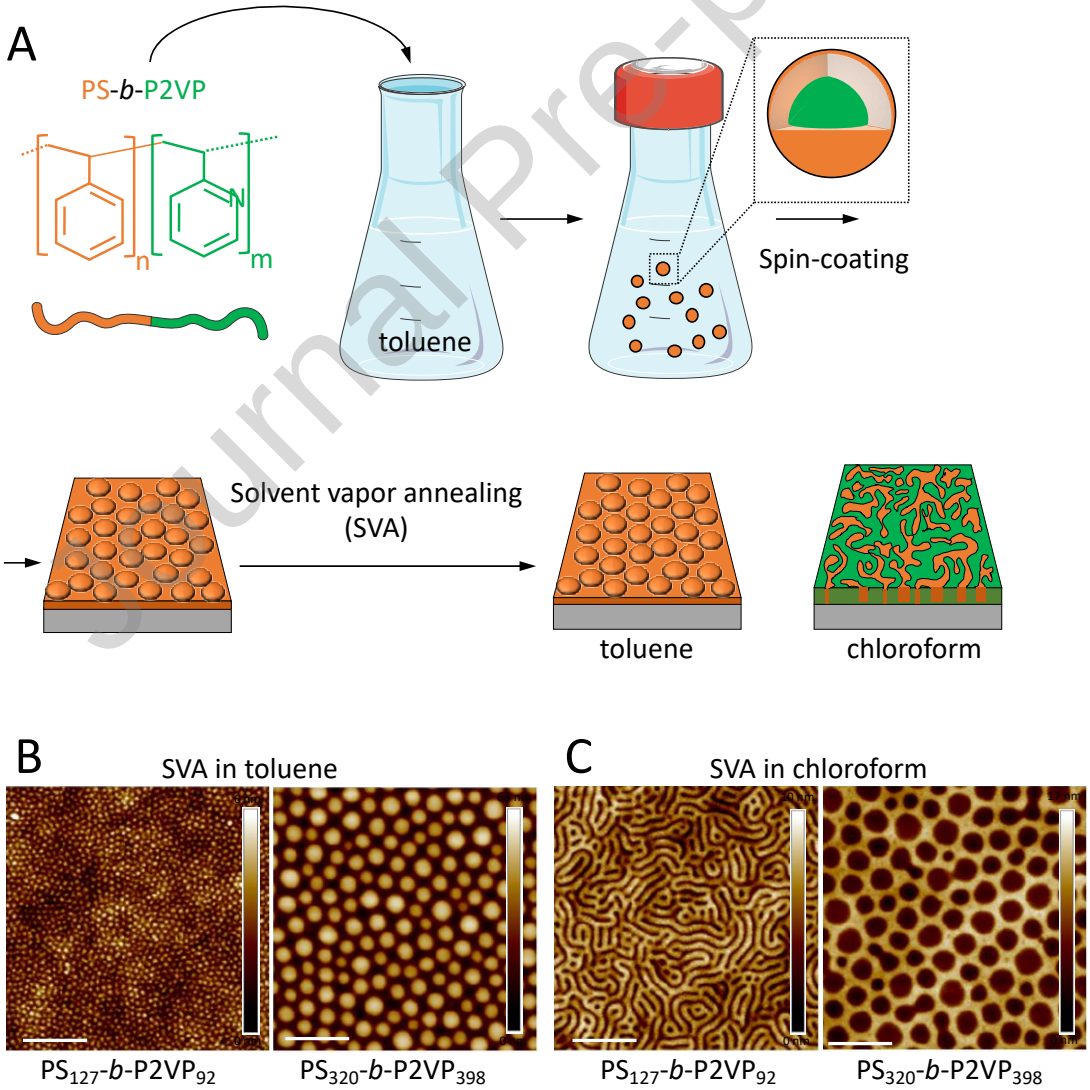

Figure 1. (A) Schematic presentation of the used methodology for assembly of nanopatterns from polystyrene-*block*-poly(2-vinyl pyridine) (PS-*b*-P2VP). (B, C) Atomic Force Microscopy (AFM) images of the nanopatterns obtained by (B) solvent vapor annealing (SVA) in toluene from PS_{127}-*b*-$P2VP_{92}$ and PS_{320}-*b*-$P2VP_{398}$ and (C) after SVA in chloroform from the same copolymers. Scale bars correspond to 500 nm.

3.2. Number of adhered cells: BMMSCs vs SaOS-2

The number of adherent cells during the first hours of contact with an implantable device, *e.g.* prothesis, is crucial for the device integration and fixation. When BMMSC were used, we observed similar number of adherent cells on all patterns and the control substrate (TCPS, red dotted line in Fig. 2) for the studied period (up to 24 h). In the case of SaOS-2, the number of adherent cells was also similar between the different patterns but the general trend was lower when compared to BMMSC (Fig. 2). Moreover, we observed an accentuated tendency of decreased number of adherent SaOS-2 after 24 h of culture. Of note, this decrease is not associated with pattern vanishing and/or eventual polymer degradation: we and others have confirmed the topography integrity at physiological conditions [24, 31, 32]. Lack of serum can be one of the reasons for this decrease because we observed a similar tendency for the control substrates (Fig. S1), although less accentuated. However, the serum absence is not the only cause because the data indicated different response of the studied cells to the nanopatterns: the preferential adhesion of BMMSC over SaOS-2 on an implant is advantageous when considering a scenario of bone regeneration after osteosarcoma, in which BMMSC are crucial for bone formation around implants and play an important role in promoting osseointegration.[32] To confirm the difference between BMMSC and SaOS-2, we performed a morphometric analysis of the adherent cells during the first 24 h of culture. This short culture time was chosen to reveal the initial response to an implanted device that is crucial for the following regeneration process.

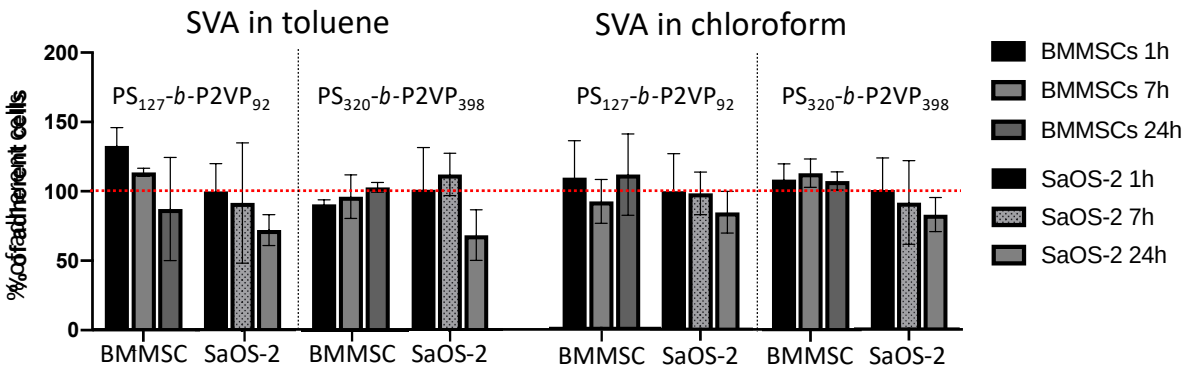

Figure 2. Percentage of BMMSCs and SaOS-2 adherent on the developed nanopatterns at different timepoints. The data was normalized by the TCPS (100%, red dotted line). No statistically significant differences between the studied conditions were observed.

3.3. Morphometric analysis

The morphology of the BMMSC and SaOS-2 cultured on the nanopatterns was visualized by staining of cells cytoskeleton and fluorescence microscopy imaging. At the first hour of culture, BMMSC on control and nanopatterned substrates had similar star-like shape with few short cellular protrusions (lamellipodia and filopodia) (Fig. 3). Longer culture times, *i.e.* 7 and 24 h, led to cells spreading and BMMSC with elongated spindle like shape and numerous filopodia and lamellipodia were observed. Of note, after 7 h of culture BMMSC on the nanotopographies had clearly defined stress fibers with parallel orientation, while BMMSC on the control TCPS substrates had disorganized and shorter stress fibers even after 24 h of culture (Fig. 3). Stress fibers are tension-generating, load-bearing mechanosensitive structures, whose formation reflects BMMSC response to the external environment: the presence of stress fibers is often correlated with strong cell adhesion to the substrate. This response can be associated with expression of soluble factors that drive actin assembly and disassembly and also with substrate surface properties such as rigidity and topography.[33]

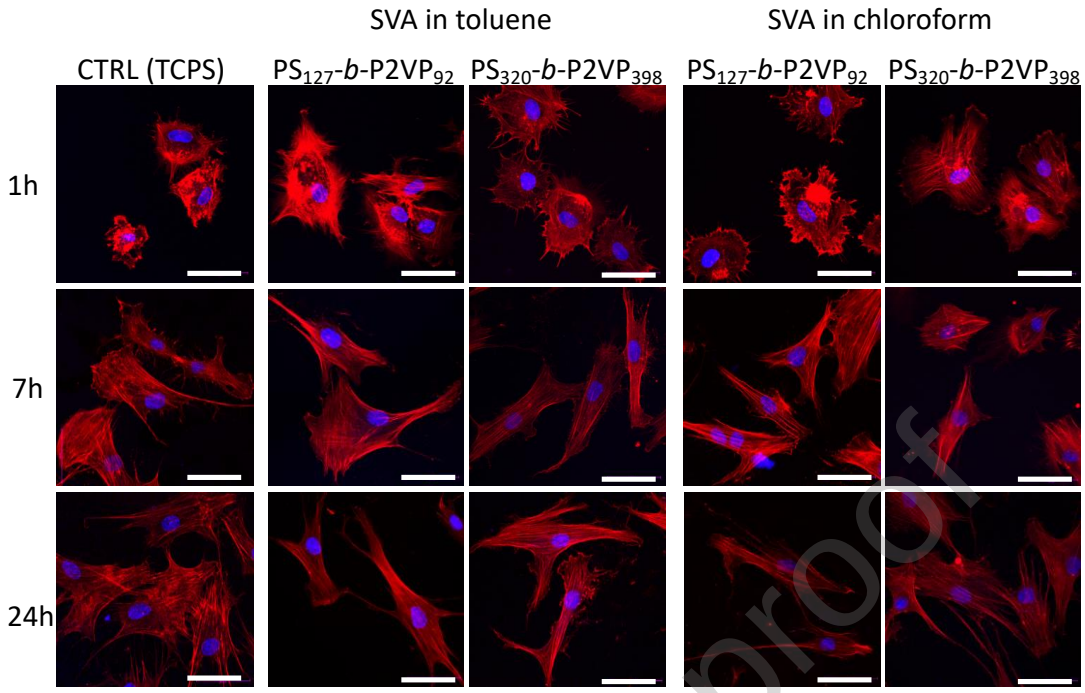

Figure 3. Representative confocal microscopy images of BMMSC cultured on the developed nanopatterns and control (CTRL) substrate (tissue culture polystyrene, TCPS). Cytoskeleton is stained with phalloidin-TRITC (red) and nucleus with DAPI (blue). Scale bars = 50 μm.

SaOS-2 had different morphology: after 1 h of culture, these cells were rounder than BMMSC and had less filopodia (Fig. 4). In the following hours these cells acquired a polygonal shape and some filopodia were visible. Short and disoriented actin stress fibers were observed for SaOS-2 on TCPS substrates, while some cells on nanopatterned substrates had stress fibers but mostly at the cells periphery. The lack of stress fibers is usually associated with migratory phenotypes[34-36], which can be the case of SaOS-2 on the studied substrates. Of note, for the studied period, we did not observe vinculin expression and focal adhesions (data not shown), which agrees with previous studies that report absence of these structures in FBS deprived medium for short culture times, *i.e.* at culture conditions similar to the used herein.[37]

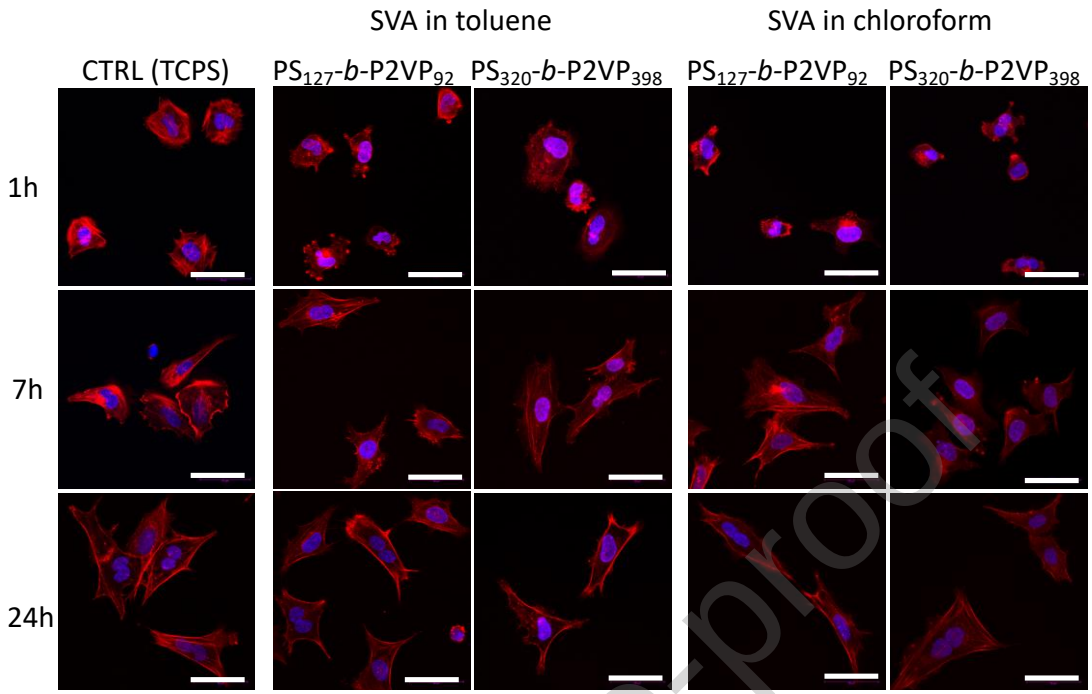

Figure 4. Representative confocal microscopy images of SaOS-2 cultured on the BCP nanopatterns and control substrate (TCPS). Cytoskeleton was stained with phalloidin (red) and nucleus with DAPI (blue). Scale bars = 50 μm.

To assess quantitatively the morphology of the cells on the developed patterns and differences among them, we performed morphometric analysis using the following parameters: area, perimeter, aspect ratio (AR) and circularity. Because of the BMMSC heterogeneity, we have analyzed a large number of cells (>2000 cells per sample) to guarantee the data representativity – an issue that has not been considered in previous studies with BMMSC on block copolymers nanopatterns.[23] The morphometric data for BMMSC (Fig. 5) showed significant differences between cells cultured on control substrates and nanopatterned surfaces: the parameters indicated faster BMMSC spreading on the nanopatterns in comparison with TCPS for the shorter culture times (1 and 7 h).

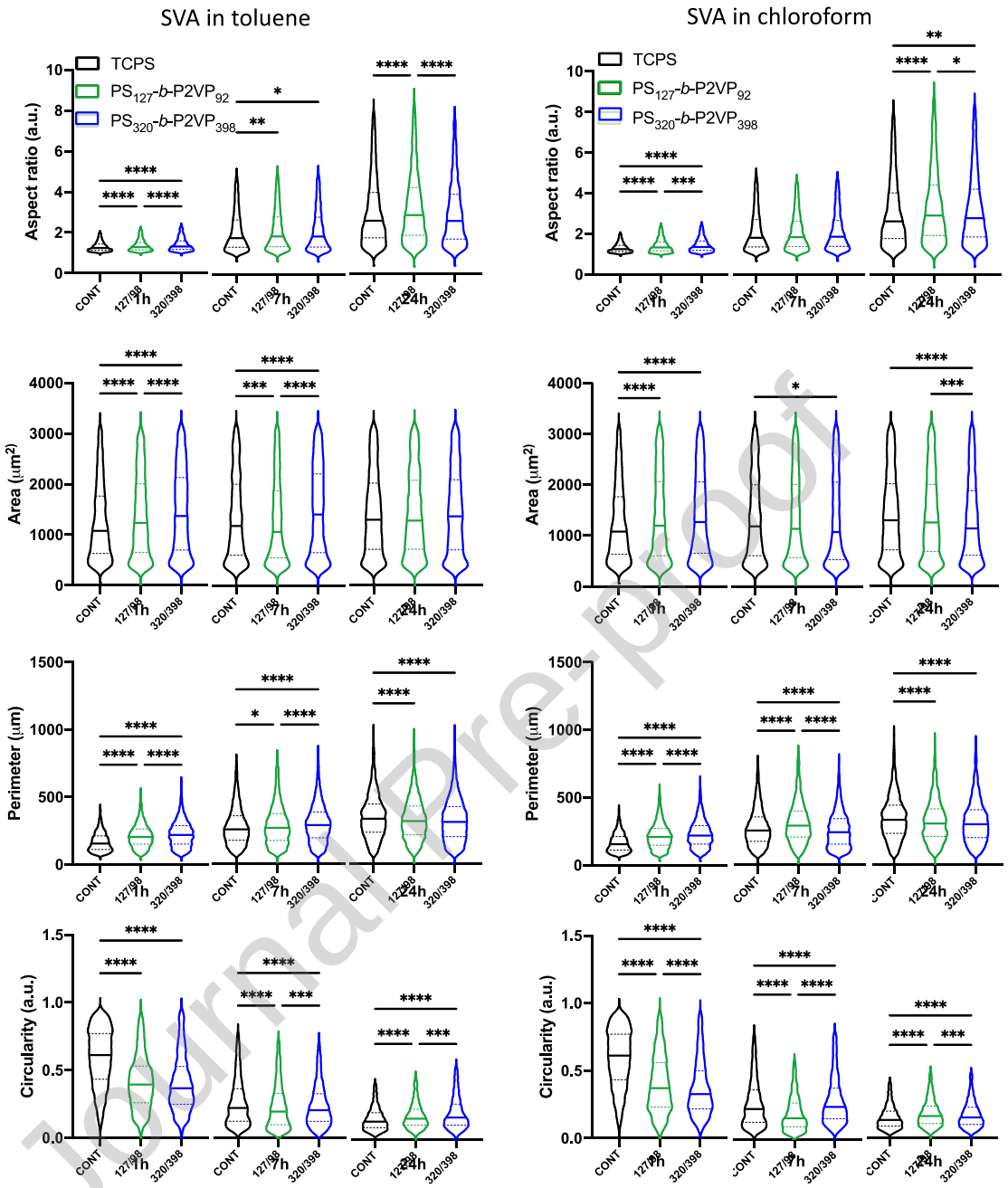

Figure 5. Morphometric data for BMMSC cultured on the developed nanopatterns and on a control substrate (TCPS). Continuous bold line represents the median and the dotted line the higher and the lower quartile. Symbols represent the statistically significant differences in relation to TCPS: *p <0.1, **p<0.01, ***p<0.001, ****p<0.0001.

Although the observed differences are generally small, they were more pronounced at the first hour and for the nanopatterns obtained with the high

molecular weight BCP (PS_{320}-*b*-$P2VP_{398}$) with either SVA solvent (chloroform and toluene). Because of the large number of cells and the high heterogeneity, we have analyzed the obtained data by principal component analysis (PCA) in order to assess the influence of the block copolymer molecular weight and the topography of the patterns on the cells morphology. For the PCA analysis, we included two extra morphometric parameters that can be obtained from the original data, surface-area (SA) and fractal dimension of cellular contour (FDC). The principal component 1 and 2 (PC1 and PC2) account for more than 95% of the variation of the BMMSC population (Table S2) with perimeter, AR, FDC, SA and circularity contributing to PC1, and PC2 being mainly affected by the area (Table S2). Using a two-dimensional (2D) PCA biplot, three clusters were distinguished based on timeframe analysis of the cells' morphology (Fig. 6). At the first hour of culture, BMMSC on the nanopatterned surfaces are clearly distinguished from the cells on TCPS controls by their higher area and lower circularity, evidencing faster adhesion on the developed nanopatterns. At this initial timepoint and during the whole studied period, BMMSC on the micellar nanopattern (SVA in toluene) obtained from the higher molecular weight copolymer PS_{320}-*b*-$P2VP_{398}$ stand from the cells on the other nanopatterned surfaces (Fig. 6). After 7 h of culture, the area (and to less extent SA and FDC) distinguishes BMMSC on TCPS and micellar PS_{320}-*b*-$P2VP_{398}$ nanopattern from the cells on the other nanopatterns that have smaller area. At the end of the studied period, smaller differences between BMMSC on different substrates were observed. Of note, at this time point the patterns generated from PS_{320}-*b*-$P2VP_{398}$ induced opposite behavior with micellar nanopatterns promoting cells spreading (compared to the control TCPS) contrary to the nanopatterns generated by SVA in chloroform. These results agree with previous data showing that BMMSC respond to nanofeatures as small as 10 nm[38, 39] and that nanostructured surfaces can promote cell adhesion.[40-43] The generally accepted mechanism explaining these results is the higher surface area and the dimensional match between the substrate nanofeatures on one side and the adhesion proteins and the cell membrane receptors on the other side. Our results agree with this mechanism: at the first hour of culture, the nanopatterns generated from PS_{320}-*b*-$P2VP_{398}$ with higher molecular weight that assembles in larger micelles (Table 1) have a closer dimensional match and therefore promote a better adhesion.

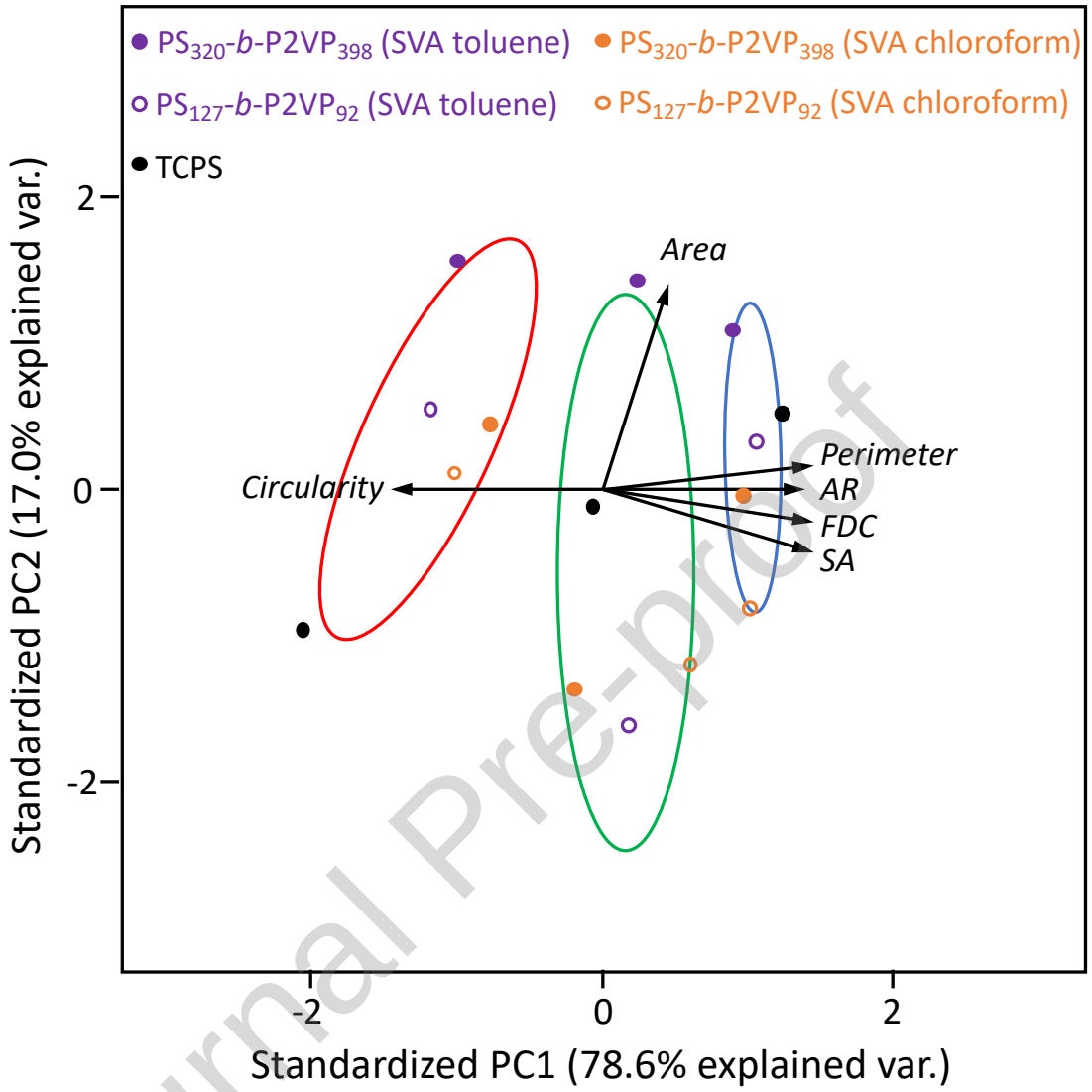

Figure 6. Biplot of the scores of the principal components (PC1, PC2) for morphometric parameters of BMMSC cultured on the different surfaces for 1 (red), 7 (green) and 24 (blue) hours. Loadings are represented as vectors (black) and correspond to the analyzed variables. Grouping can be observed between the different surfaces for each timepoint based on its factorial scores.

We have also performed morphometric analysis of the osteosarcoma cell line SaOS-2 in contact with TCPS control and BCP nanopatterns (Fig. 7). At the initial period, SaOS-2 spreading is also faster for the nanopatterns (except for the ones assembled from PS_{127}-*b*-$P2VP_{92}$) when compared to the control substrates but the difference is

smaller than the determined for BMMSC. This tendency is inverted after 24 h of culture, when a higher spreading of SaOS-2 is observed on the control substrates.

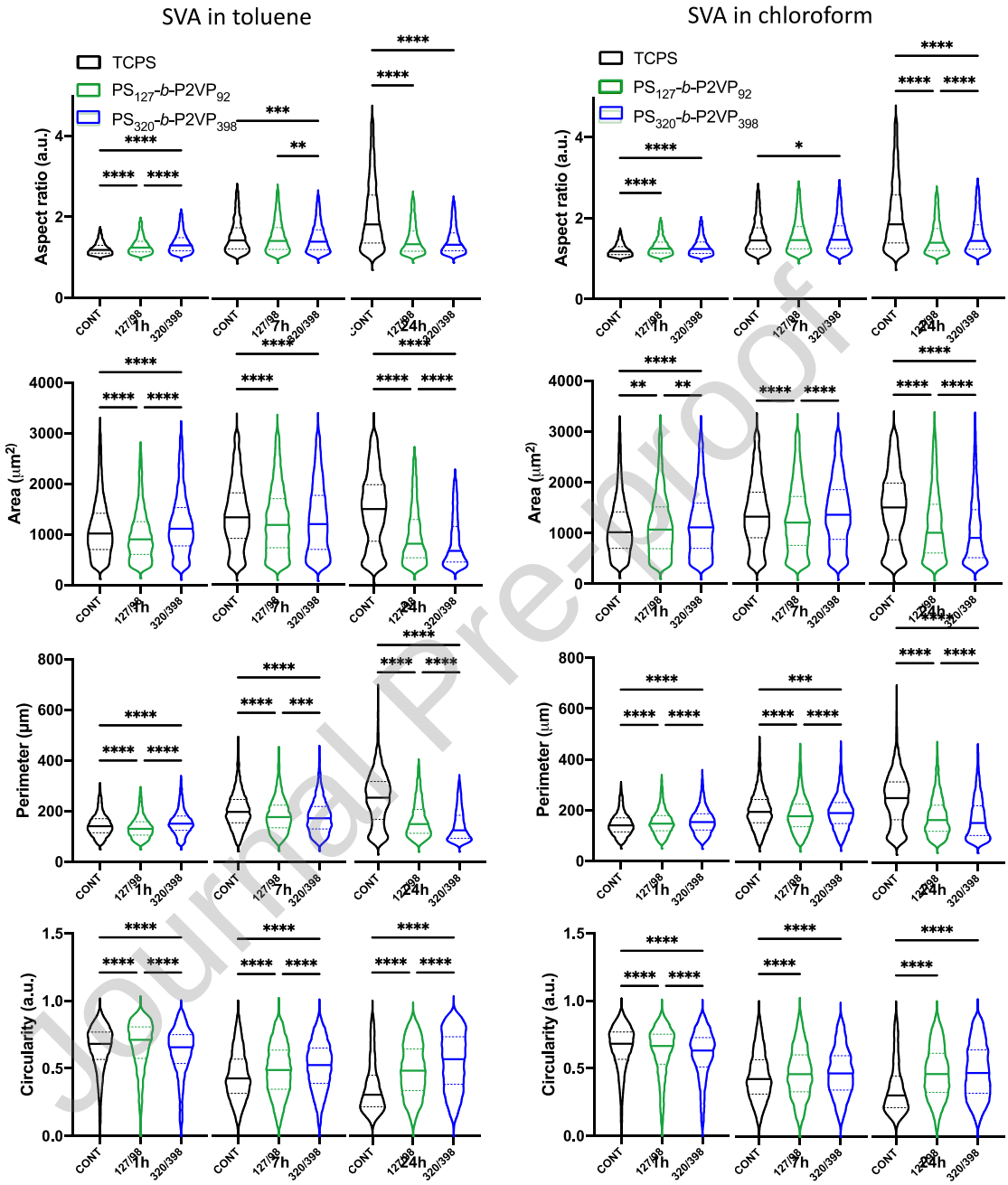

Figure 7. Morphometric data for SaOS-2 cultured on the developed nanopatterns and control (TCPS) substrates for 1, 7, and 24 h. Continuous bold line represents the median and the doted line the higher and the lower quartile. Symbols represent the statistically significant differences in relation to TCPS: *p <0.1, **p<0.01, ***p<0.001, ****p<0.0001.

The PCA of SaOS-2 with perimeter, AR, FDC and circularity contributing to PC1, and area and SA to PC2 (Table 3) showed very similar morphometric parameters for SaOS-2 on different substrates after 1 and 7 h (Fig. 8). After 24 h the scenario is completely different, with SaOS-2 spreading much more on TCPS than in the nanopatterned surfaces.

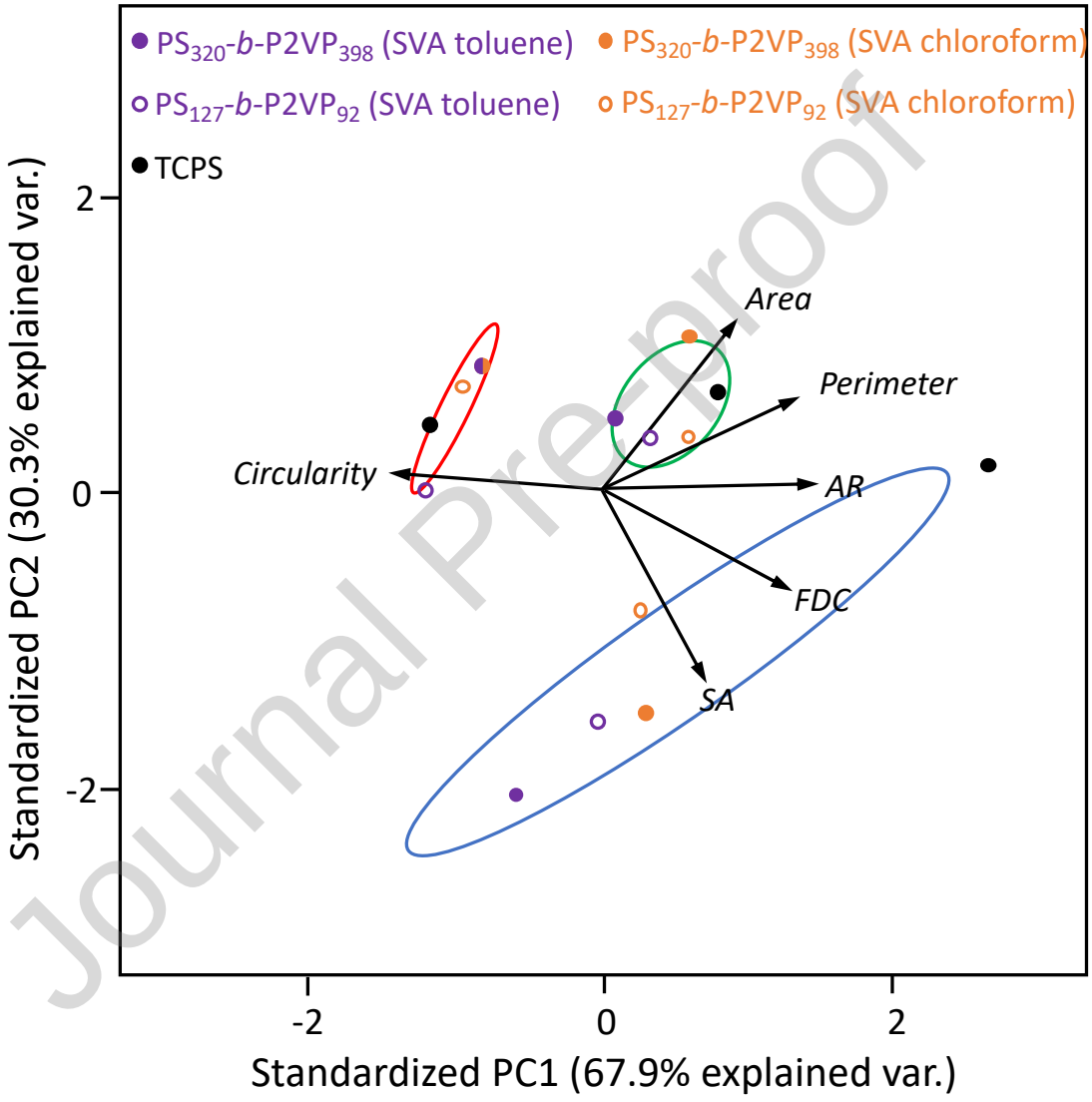

Figure 8. Biplot of the scores of the principal components (PC1, PC2) for morphometric parameters of SaOS-2 cultured on the studied substrates and TCPS controls for 1 (red), 7 (green), and 24 (blue) hours. Loadings vectors (black) correspond to the analyzed variables. Grouping can be observed between the different surfaces for each timepoint based on its factorial scores.

A comparison of the PCA biplots for BMMSC and SaOS-2 shows different effect of the developed nanopatterns on these cells. The nanopatterns promote the adhesion and spreading of BMMSC when compared to TCPS but this effect is not observed for SaOS-2. Of note is the effect of the micellar nanopattern obtained by SVA in toluene of PS_{320}-*b*-$P2VP_{398}$ that had greatest but opposite effect on the studied cells after 24 h: this pattern arrested the spreading of the osteosarcoma cell line but promoted the adhesion and spreading of BMMSC. The observed arrest of SaOS-2 spreading can be associated with a migratory phenotype in contrast with the strong BMMSC adhesion concomitant with the formation of long stress fibers (Fig. 3). This different behavior can be explained with the different integrin subunits involved in BMMSCs and SaOS-2 adhesion and with the secretion of different adhesive matrix molecules (fibronectin, vitronectin).[44, 45]

BMMSCs and SaOS-2 differentiation strongly depends on the biomaterial's surface properties, which is directly related to the amount and conformation of the proteins deposited on the surfaces.[46] [47] Given the fact that we used serum deprived medium, at 1h, the cells are interacting directly with the surface, being, therefore, affected by its chemical and physical properties. However, after 24 h, cells have already secreted proteins to the ECM and this ECM-coated nanopattern results in a different cell/biomaterial response.

This nanopattern can be used in different clinical scenarios. Metal implants are commonly used to support the bone after fracture during the healing process. A coating of these implants by assembly of PS_{320}-*b*-$P2VP_{398}$ and SVA in toluene can enhance bone remodeling and regeneration because BMMSC are crucial players in these processes as the first intervenient.[49] Considering an osteosarcoma scenario, the fast BMMSC adhesion and spreading together with the arrest of SaOS-2 spreading and its association with a migratory phenotype will be beneficial for bone regeneration after removal of the damaged tissue and avoiding cancer recurrence.

4. Conclusions

We demonstrated that the chemistry and the topography of PS-*b*-P2VP nanopatterns influence cell adhesion and morphology. Importantly, these results were obtained by an analysis of a high number of cells and nanopatterns with different sizes, not considered previously.[23] The developed nanopatterns have a distinct effect on the two studied cell types: in particular micellar nanopatterns assembled from PS_{320}-*b*-$P2VP_{398}$ promote the adhesion and spreading of BMMSC and arrested these processes for the osteosarcoma cell line SaOS-2. These results together with the previous data showing bactericidal properties of these patterns [24] demonstrate the potential of BCP self-assembly for coating of bone implants that promote the regeneration process and suppress the tumor growth/recurrence towards bone healing. The next step in the validation of these coatings will be their assessment in complex and dynamic bioenvironments.

CRediT authorship contribution statement

Raúl Fontelo: Conceptualization, methodology, verification, formal analysis, investigation, writing original draft and visualization. Diana Soares da Costa: Methodology, validation, and investigation. Rui L Reis: Supervision, resources, and funding acquisition. Ramón Novoa-Carballal and Iva Pashkuleva: Conceptualization, methodology, writing & editing, supervision, project administration, and funding acquisition.

Declaration of Competing Interest

☒ The authors declare that they have no known competing financial interests or personal relationships that could have appeared to influence the work reported in this paper.

☐The authors declare the following financial interests/personal relationships which may be considered as potential competing interests:

Acknowledgments

Portuguese Foundation for Science and Technology for the grants PTDC/QUI-POL/28117/2017, PD/BD/128085/2016, and CEECIND/00814 /2017.

References

[1] S. Huang, D.E. Ingber, The structural and mechanical complexity of cell-growth control, Nat Cell Biol 1(5) (1999) E131-E138.
[2] R. Ungai-Salanki, B. Peter, T. Gerecsei, N. Orgovan, R. Horvath, B. Szabo, A practical review on the measurement tools for cellular adhesion force, Adv Colloid Interfac 269 (2019) 309-333.
[3] C.S. Chen, M. Mrksich, S. Huang, G.M. Whitesides, D.E. Ingber, Geometric control of cell life and death, Science 276(5317) (1997) 1425-1428.
[4] R. McBeath, D.M. Pirone, C.M. Nelson, K. Bhadriraju, C.S. Chen, Cell shape, cytoskeletal tension, and RhoA regulate stem cell lineage commitment, Dev Cell 6(4) (2004) 483-495.
[5] S. Lavenus, J.C. Ricquier, G. Louarn, P. Layrolle, Cell interaction with nanopatterned surface of implants, Nanomedicine-Uk 5(6) (2010) 937-947.
[6] X.Q. Liu, R.Z. Tang, Biological responses to nanomaterials: understanding nano-bio effects on cell behaviors, Drug Deliv 24(2) (2017) 1-15.
[7] N.I. Aminuddin, R. Ahmad, S.A. Akbar, B. Pingguan-Murphy, Osteoblast and stem cell response to nanoscale topographies: a review, Science and Technology of Advanced Materials 17(1) (2016) 698-714.

[8] A. Lagunas, A.G. Castano, J.M. Artes, Y. Vida, D. Collado, E. Perez-Inestrosa, P. Gorostiza, S. Claros, J.A. Andrades, J. Samitier, Large-scale dendrimer-based uneven nanopatterns for the study of local arginine-glycine-aspartic acid (RGD) density effects on cell adhesion, Nano Res 7(3) (2014) 399-409.
[9] S. Jaehrling, K. Thelen, T. Wolfram, G.E. Pollerberg, Nanopatterns Biofunctionalized with Cell Adhesion Molecule DM-GRASP Offered as Cell Substrate: Spacing Determines Attachment and Differentiation of Neurons, Nano Lett 9(12) (2009) 4115-4121.
[10] E.A. Cavalcanti-Adam, A. Micoulet, J. Blummel, J. Auernheimer, H. Kessler, J.P. Spatz, Lateral spacing of integrin ligands influences cell spreading and focal adhesion assembly, Eur J Cell Biol 85(3-4) (2006) 219-224.
[11] V.C. Hirschfeld-Warneken, M. Arnold, A. Cavalcanti-Adam, M. Lopez-Garcia, H. Kessler, J.P. Spatz, Cell adhesion and polarisation on molecularly defined spacing gradient surfaces of cyclic RGDfK peptide patches, Eur J Cell Biol 87(8-9) (2008) 743-750.
[12] M. Arnold, E.A. Cavalcanti-Adam, R. Glass, J. Blummel, W. Eck, M. Kantlehner, H. Kessler, J.P. Spatz, Activation of integrin function by nanopatterned adhesive interfaces, Chemphyschem 5(3) (2004) 383-388.
[13] R.I. Sharma, J.G. Snedeker, Biochemical and biomechanical gradients for directed bone marrow stromal cell differentiation toward tendon and bone, Biomaterials 31(30) (2010) 7695-7704.
[14] A.V. Taubenberger, M.A. Woodruff, H.F. Bai, D.J. Muller, D.W. Hutmacher, The effect of unlocking RGD-motifs in collagen I on pre-osteoblast adhesion and differentiation, Biomaterials 31(10) (2010) 2827-2835.
[15] R. Ayala, C. Zhang, D. Yang, Y. Hwang, A. Aung, S.S. Shroff, F.T. Arce, R. Lal, G. Arya, S. Varghese, Engineering the cell-material interface for controlling stem cell adhesion, migration, and differentiation, Biomaterials 32(15) (2011) 3700-3711.
[16] S.J. Yeon, J.W. Lee, J.W. Lee, E.J. Jeong, Y.J. Kwark, S.H. Kim, K.Y. Lee, Responses of preosteoblasts on nano-structured polymer surfaces prepared from block copolymer-surfactant complexes, Soft Matter 8(30) (2012) 3898-3903.
[17] E. Lamers, X.F. Walboomers, M. Domanski, J. te Riet, F.C.M.J.M. van Delft, R. Luttge, L.A.J.A. Winnubst, H.J.G.E. Gardeniers, J.A. Jansen, The influence of nanoscale grooved substrates on osteoblast behavior and extracellular matrix deposition, Biomaterials 31(12) (2010) 3307-3316.
[18] S. Dobbenga, L.E. Fratila-Apachitei, A.A. Zadpoor, Nanopattern-induced osteogenic differentiation of stem cells - A systematic review, Acta Biomater 46 (2016) 3-14.
[19] H.L. Zhang, X.W. Zheng, W. Ahmed, Y.J. Yao, J. Bai, Y.C. Chen, C.Y. Gao, Design and Applications of Cell -Selective Surfaces and Interfaces, Biomacromolecules 19(6) (2018) 1746-1763.
[20] L. Csaderova, E. Martines, K. Seunarine, N. Gadegaard, C.D.W. Wilkinson, M.O. Riehle, A Biodegradable and Biocompatible Regular Nanopattern for Large-Scale Selective Cell Growth, Small 6(23) (2010) 2755-2761.
[21] H. Ozcelik, C. Padeste, V. Hasirci, Systematically organized nanopillar arrays reveal differences in adhesion and alignment properties of BMSC and Saos-2 cells, Colloid Surface B 119 (2014) 71-81.
[22] Y. Mai, A. Eisenberg, Self-assembly of block copolymers, Chem Soc Rev 41(18) (2012) 5969-85.

[23] H.L. Khor, Y. Kuan, H. Kukula, K. Tamada, W. Knoll, M. Moeller, D.W. Hutmacher, Response of cells on surface-induced nanopatterns: Fibroblasts and mesenchymal progenitor cells, Biomacromolecules 8(5) (2007) 1530-1540.
[24] R. Fontelo, D.S. da Costa, R.L. Reis, R. Novoa-Carballal, I. Pashkuleva, Bactericidal nanopatterns generated by block copolymer self-assembly, Acta Biomater 112 (2020) 174-181.
[25] M. Shafiq, Y. Jung, S.H. Kim, Insight on stem cell preconditioning and instructive biomaterials to enhance cell adhesion, retention, and engraftment for tissue repair, Biomaterials 90 (2016) 85-115.
[26] S. Lee, E. Choi, M.J. Cha, K.C. Hwang, Cell Adhesion and Long-Term Survival of Transplanted Mesenchymal Stem Cells: A Prerequisite for Cell Therapy, Oxid Med Cell Longev 2015 (2015).
[27] C.R. Pedrosa, D. Arl, P. Grysan, I. Khan, S. Durrieu, S. Krishnamoorthy, M.C. Durrieu, Controlled Nanoscale Topographies for Osteogenic Differentiation of Mesenchymal Stem Cells, Acs Appl Mater Inter 11(9) (2019) 8858-8866.
[28] A. Vilaca, R.M.A. Domingues, H. Tiainen, B.B. Mendes, A. Barrantes, R.L. Reis, M.E. Gomes, M. Gomez-Florit, Multifunctional Surfaces for Improving Soft Tissue Integration, Adv Healthc Mater 10(8) (2021).
[29] D.A. Rennerfeldt, K.J. Van Vliet, Concise Review: When Colonies Are Not Clones: Evidence and Implications of Intracolony Heterogeneity in Mesenchymal Stem Cells, Stem Cells 34(5) (2016) 1135-1141.
[30] C. Jin, B.C. Olsen, E.J. Luber, J.M. Buriak, Nanopatterning via Solvent Vapor Annealing of Block Copolymer Thin Films, Chem Mater 29(1) (2017) 176-188.
[31] R. Fontelo, D. Soares da Costa, R.L. Reis, R. Novoa-Carballal, I. Pashkuleva, Antithrombotic and hemocompatible properties of nanostructured coatings assembled from block copolymers, J. Colloid Interface Sci. 608 (2022) 1608-1618.
[32] G. Yang, W. Fang, T. Liu, F. He, X. Chen, Y. Zhou, X. Guan, Gene expression profiling of bone marrow-derived stromal cells seeded onto a sandblasted, large-grit, acid-etched-treated titanium implant surface: The role of the Wnt pathway, Arch Oral Biol 61 (2016) 71-8.
[33] K. Burridge, E.S. Wittchen, The tension mounts: stress fibers as force-generating mechanotransducers, J Cell Biol 200(1) (2013) 9-19.
[34] I.M. Herman, N.J. Crisona, T.D. Pollard, Relation between cell activity and the distribution of cytoplasmic actin and myosin, The Journal of Cell Biology 90 (1981) 84-91.
[35] X. Trepat, Z. Chen, K. Jacobson, Cell migration, Compr Physiol 2(4) (2012) 2369-92.
[36] K. Burridge, Are stress fibres contractile?, Nature 294 (1981) 691-692.
[37] M. Verdanova, P. Sauerova, U. Hempel, M.H. Kalbacova, Initial cell adhesion of three cell types in the presence and absence of serum proteins, Histochem Cell Biol 148(3) (2017) 273-288.
[38] M.J. Dalby, D. McCloy, M. Robertson, H. Agheli, D. Sutherland, S. Affrossman, R.O. Oreffo, Osteoprogenitor response to semi-ordered and random nanotopographies, Biomaterials 27(15) (2006) 2980-7.
[39] M.J. Dalby, D. McCloy, M. Robertson, C.D. Wilkinson, R.O. Oreffo, Osteoprogenitor response to defined topographies with nanoscale depths, Biomaterials 27(8) (2006) 1306-15.

[40] A. Broz, V. Baresova, A. Kromka, B. Rezek, M. Kalbacova, Strong influence of hierarchically structured diamond nanotopography on adhesion of human osteoblasts and mesenchymal cells, Phys Status Solidi A 206(9) (2009) 2038-2041.
[41] M.S. Mozumder, J. Zhu, H. Perinpanayagam, Titania-polymeric powder coatings with nano-topography support enhanced human mesenchymal cell responses, J Biomed Mater Res A 100a(10) (2012) 2695-2709.
[42] Y. Hou, W.Y. Xie, L.X. Yu, L.C. Camacho, C.X. Nie, M. Zhang, R. Haag, Q. Wei, Surface Roughness Gradients Reveal Topography-Specific Mechanosensitive Responses in Human Mesenchymal Stem Cells, Small 16(10) (2020).
[43] K. Anselme, M. Bigerelle, Statistical demonstration of the relative effect of surface chemistry and roughness on human osteoblast short-term adhesion, J Mater Sci-Mater M 17(5) (2006) 471-479.
[44] K.L. Kilpadi, A.A. Sawyer, C.W. Prince, P.L. Chang, S.L. Bellis, Primary human marrow stromal cells and Saos-2 osteosarcoma cells use different mechanisms to adhere to hydroxylapatite (vol 68A, pg 273, 2005), J Biomed Mater Res A 73a(2) (2005) 254-254.
[45] S. Vohra, K.M. Hennessy, A.A. Sawyer, Y. Zhuo, S.L. Bellis, Comparison of mesenchymal stem cell and osteosarcoma cell adhesion to hydroxyapatite, J Mater Sci-Mater M 19(12) (2008) 3567-3574.
[46] T. Razafiarison, C.N. Holenstein, T. Stauber, M. Jovic, E. Vertudes, M. Loparic, M. Kawecki, L. Bernard, U. Silvan, J.G. Snedeker, Biomaterial surface energy-driven ligand assembly strongly regulates stem cell mechanosensitivity and fate on very soft substrates, Proc. Nat. Acad. Sci. U.S.A. 115(18) (2018) 4631-4636.
[47] T. Razafiarison, U. Silván, D. Meier, J.G. Snedeker, Surface-Driven Collagen Self-Assembly Affects Early Osteogenic Stem Cell Signaling, Advanced Healthcare Materials 5(12) (2016) 1481-1492.
[48] R.K. Sironen, M. Tammi, R. Tammi, P.K. Auvinen, M. Anttila, V.M. Kosma, Hyaluronan in human malignancies, Exp Cell Res 317(4) (2011) 383-91.
[49] M.N. Knight, K.D. Hankenson, Mesenchymal Stem Cells in Bone Regeneration, Adv Wound Care (New Rochelle) 2(6) (2013) 306-316.

Highlights

- Six morphometric descriptors were investigated by principal component analysis in more than > 2000 cells per condition.
- Nanopattern surface chemistry and topography influence cell adhesion and morphology.
- Micellar nanopatterns promote the spreading of BMMSC but arrest these processes for the osteosarcoma cells